Recent progress of plasma exhaust concepts and divertor designs for tokamak DEMO reactors

Nuclear Materials and Energy 35 (2023) 101446

Contents lists available at ScienceDirect

Nuclear Materials and Energy

journal homepage: www.elsevier.com/locate/nme

Recent progress of plasma exhaust concepts and divertor designs for tokamak DEMO reactors

N. Asakura [a,*], K. Hoshino [b], S. Kakudate [a], F. Subba [c], J.-H. You [d], S. Wiesen [e], T.D. Rognlien [f], R. Ding [g], S. Kwon [h]

[a] National Institutes for Quantum Science and Technology (QST), Naka, Ibaraki 311-0193 Japan
[b] Graduate School of Science and Technology, Keio University, Yokohama 223-8522, Japan
[c] NEMO Group, Politecnico di Torino, Torino, Italy
[d] Max Planck Institute for Plasma Physics, Boltzmannstrasse 2, Garching, Germany
[e] Forschungszentrum Jülich GmbH, Institut für Energie und Klimaforschung Plasmaphysik, 52425 Jülich, Germany
[f] Lawrence Livermore National Laboratory, Livermore, CA, 94551, USA
[g] Institute of Plasma Physics, Chinese Academy of Sciences, Hefei 230031, China
[h] Korea Institute of Fusion Energy, Daejeon 34133, Republic of Korea

ARTICLE INFO

Keywords:
DEMO
Power exhaust
Divertor simulation
Divertor design
Water-cooled divertor

ABSTRACT

The power exhaust concept and an appropriate divertor design are common critical issues for tokamak DEMO design activities which have been carried out in Europe, Japan, China, Korea and the USA. Conventional divertor concepts and power exhaust studies for recent DEMO designs (P_{fusion} = 1 – 2 GW, R_p = 7 – 9 m) are reviewed from the viewpoints of the plasma physics issues and the divertor engineering design. Radiative cooling is a common approach for the power fusion scenario. Requirements on the main plasma radiation fraction ($f_{rad}^{main} = P_{rad}^{main}/P_{heat}$) and the plasma performance constrain the divertor design concept. Different challenges contribute to optimizing the future DEMO designs: for example, (i) increasing the main plasma radiation fraction for ITER-level P_{sep}/R_p designs and simplifying the divertor geometry, and (ii) extending ITER divertor geometry with increasing divertor radiation (P_{rad}^{div}) for larger $P_{sep}/R_p \geq 25 MWm^{-1}$ designs. Power exhaust simulations with large P_{sep} = 150 – 300 MW have been performed using integrated divertor codes considering an ITER-based divertor geometry with longer leg length (1.6 – 1.7 m), as in a common baseline design. Geometry effects (ITER like geometry or more open one without baffle) on the plasma detachment profile and the required divertor radiation fraction ($f_{rad}^{div} = P_{rad}^{div}/P_{sep}$) were key aspects of these studies. All simulations showed that the divertor plasma detachment were extended widely across the target plate with a reduction in the peak heat load of $q_{target} \leq 10$ MWm^{-2} for the large f_{rad}^{div} = 0.7 – 0.8, while the peak q_{target} location and value were noticeably different in the partially detached divertor. Simulation results also demonstrated that radial diffusion coefficients of the heat and particle fluxes were critical parameters for DEMO divertor design, and that effects of plasma drifts on outboard-enhanced asymmetry of the heat flux, suggested the need for longer divertor leg to ensure the existence of a detached divertor operation with $q_{target} \leq 10$ MWm^{-2}.

Integrated design of the water cooled divertor target, cassette body (CB) and cooling pipe routing has been developed for each DEMO concept, based on the ITER-like tungsten monoblock (W-MB) with Cu-alloy cooling pipes. Engineering design adequate under higher neutron irradiation condition was required. Therefore, inlet coolant temperature (T_{cool}) was increased. In current designs, it still shows a large potential variation between 70 °C and 200 °C. The influence of thermal softening on the Cu-alloy (CuCrZr) pipe was fostered near the strike-point when the high q_{target} of ~10 MWm^{-2} was studied. Improved technologies for high heat flux components based on the ITER W-MB unit have been developed for EU-DEMO. Different coolant conditions (low- and high-T_{cool}) were provided for Cu-alloy and reduced activation ferritic martensitic (RAFM) steel heat sink units, respectively. The high-T_{cool} coolant was also considered for the CB and supporting structures. Appropriate conditions for the high-T_{cool} coolant, i.e. 180 °C/ 5 MPa (EU-DEMO) and 290 °C/ 15 MPa (JA-DEMO, CFETR and K-DEMO), will be determined in the future optimizations of the divertor and DEMO design.

* Corresponding author at: Plasma Theory and Simulation Group, Naka Fusion Institute, QST, 801-1 Mukoyama, Naka, Ibaraki 311-0193, Japan.
E-mail address: asakura.nobuyuki@qst.go.jp (N. Asakura).

https://doi.org/10.1016/j.nme.2023.101446
Received 17 October 2022; Received in revised form 10 April 2023; Accepted 11 May 2023
Available online 15 May 2023

1. Introduction

Demonstration of electric power production larger than internal power consumption (net electricity generation) is the most outstanding challenge of a DEMO fusion reactor. The fusion power (P_{fusion}) and device size (major radius: R_p) are increased to achieve net electricity generation and tritium breeding to sustain the fusion reactions (self-sufficient tritium breeding). Power exhaust concept and the appropriate divertor design are common critical issues for DEMO tokamak development activities, which have been carried out in Europe (EU-DEMO1 [1,2], Flexi-DEMO [3]), Japan (JA-DEMO 2014 [4,5] and high plasma elongation: high-κ [6]), China (CFETR [7]), Korea (K-DEMO [8,9]), and the USA (FNSF [10], ARIES-ACT1 [11]). Representative plasma parameters and heating power of recent DEMO concepts are shown in Table 1. Those for ITER [12,13] are also added. These plasma parameters are referred to in their cited references. Noted that results of the power exhaust and divertor design in this paper may be taken from other related references, where some design parameters can differ slightly from those representative ones. The EU-DEMO1 baseline design (R_p/a_p = 9.0/2.9 m, a_p: midplane minor radius) is considered here, which is referred to as EU-DEMO in the following sections. The power handling concept of the recently proposed Flexi-DEMO (R_p/a_p = 8.4/2.71 m, aiming for not only pulsed operation but also steady-state operation if the plasma performance is improved) is similar to the baseline design. Pulsed operation performance was also investigated in the steady-state design of JA-DEMO 2014 (R_p/a_p = 8.5/2.4 m). JA-DEMO high-κ (elongation at 95% of a_p: κ_{95} = 1.75) can increase the plasma current (I_p) with the same device size (R_p and a_p), toroidal field (B_T = 5.9 T) and safety factor (q_{95} = 4.1), which is considered as a reference power exhaust concept in the following sections. For CFETR (R_p/a_p = 7.2/2.2 m) and K-DEMO (R_p/a_p = 6.8/2.2 m), plasma parameters at the first operational stage are considered. The design activity for FNSF (R_p/a_p = 4.8/1.2 m) was recently reviewed, aiming at developing sufficient engineering and technology for tritium breeding ratio (TBR ~ 1.0) and proceeding issues related to net electricity production . A power plant concept from the USA such as ARIES-ACT1 (R_p/a_p = 6.25/1.56 m) will achieve above DEMO missions.

Generally, pulsed DEMO concepts have larger P_{fusion}, and steady-state concepts must increase the auxiliary power (P_{aux}) for sufficient plasma current drive. The total heating power (P_{heat}) by α-particles (P_α) and P_{aux} of these DEMO concepts is increased to 1.8 – 3 times larger than that of ITER, while the device size (R_p) is restricted from the ITER-level to 1.5 times larger. A power exhaust parameter of P_{heat}/R_p = 39 – 62 MWm^{-1} noticeably larger than ITER (24 MWm^{-1}) suggests significant increase of the heat flux in the scrape-off layer (SOL) , if radiation losses in the main plasma (P_{rad}^{main}) are not expected. Double-null divertor design is proposed (K-DEMO, FNSF) or considered (EU-DEMO) for devices with P_{heat}/R_p larger than twice that of ITER. The power exhaust scenario and divertor design for the DEMO reactor are critical issues of physics, engineering and technology, and challenges are present even in the conventional approach based on the ITER divertor. During the conceptual design phase, it is important to review the key topics of representative DEMO divertor concepts to facilitate their future improvement and development,even though the reference design concepts of the DEMO reactor, power exhaust and divertor design differ somewhat in each community. Here, we summarize common views and differences in the divertor designs , and clarify critical issues and challenges.

First, the power exhaust scenarios in the main plasma and divertor have been investigated for the various DEMO concepts, while keeping the radiative cooling by impurity seeding as a common approach. The total radiation fraction in the main plasma and divertor is large ($f_{rad}^{tot} = P_{rad}^{tot}/P_{heat} \geq 0.8$, where $P_{rad}^{tot} = P_{rad}^{main} + P_{rad}^{sol} + P_{rad}^{div}$: total radiation loss in the main plasma, SOL and divertor), compared to that for ITER (f_{rad}^{tot} = 0.6 – 0.7) in order to reduce the peak heat load on the divertor target (q_{target}) to 10 MWm^{-2} level [12,13].

Second, power exhaust simulations in the divertor have been performed by integrated divertor simulation codes to predict a self-consistent transport solution for the plasma, neutrals and impurities in the SOL and divertor. In particular, for the reactor designs, the divertor plasma detachment is required to significantly reduce both the plasma ion and electron temperatures near the strike-points (T_i^{div}, T_e^{div}) and the peak q_{target}. Formation of divertor plasma detachment and an operational window in terms of key power exhaust parameters such as exhaust power to the SOL ($P_{sep} = P_{heat}$ - P_{rad}^{main}), radiation loss fraction in the SOL and divertor normalized by P_{sep} ($f^{*div}_{rad} = (P_{rad}^{sol} + P_{rad}^{div})/P_{sep}$), and characteristic width of the heat flux profile in SOL (λ_q^{SOL}) have been investigated to determine appropriate divertor designs [14–24]. Larger f^{*div}_{rad} is required as the divertor power handling parameter (P_{sep}/R_p) is increased compared to the ITER values (f^{*div}_{rad} = 0.5 – 0.6, P_{sep}/R_p = 16 MWm^{-1}) [25].

Third, it is also necessary to develop the foreseeable engineering design of the divertor under more severe neutron irradiation conditions compared to ITER. Integrated designs of the water cooled divertor target, cassette and cooling pipe routing have been recently developed for each DEMO concept. The plasma facing components (PFCs) in these conventional divertor designs for DEMO is mostly based on the ITER technology [26], i.e. tungsten monoblock (W-MB) concept with Cu-alloy coolant pipes. Arrangements of the PFCs and coolant pipes for the different DEMO divertor concepts, and common design issues of the water cooled divertor are summarized. Here, design concepts of single-null magnetic geometry and water-cooled divertor are the main focus. Helium (He) cooling target concept is considered for the USA DEMO

Table 1
Key design parameters of recent DEMO concepts, obtained by system codes.

Parameters	EU-DEMO [1,2]	JA-DEMO [4,5]	CFETR (1st stage) [7]	K-DEMO (1st phase) [8,9]	FNSF [10]	ITER (inductive, Q = 10) [12,13]
R_p (m)/ a_p (m)	9.0/ 2.9	8.5/ 2.4	7.2/ 2.2	6.8/ 2.1	4.8/ 1.2	6.2/ 2.0
A	3.1	3.5	3.3	3.2	3.5	3.1
I_p (MA)	18.0	12.3	13.8	12.3	7.9	14
B_T (T)/ B_T^{max} (T)	5.9/ 12.5	5.94/ 12.1	6.5/ 14	7.4/ 16	7.5/ 15.9	5.3/ 12
κ_{95}	1.6	1.65	2.0	1.8	2.1	1.7
q_{95}	3.5	4.1	5.5	7.3	6.0	3
Operation	Pulsed 2-hours	steady-state	steady-state	steady-state	steady-state	~ 400 s
Divertor configuration	Single null (option: Double null)	Single null	Single null	Double null	Double null	Single null
P_{fusion} (MW)	2000	1462	974	2200	520	500
P_{aux} (MW)	50	84	82	160	129	73 (installed)
P_{heat}: $P_\alpha + P_{aux}$ (MW)	457	376	277	600	233	~ 150
P_{heat}/R_p (MWm^{-1})	53	44	39	88	49	24
ave. neutron load to first wall (MWm^{-2})	~ 1	~ 1	~ 0.7	~ 2	~ 1.2	0.5

divertor. The double-null divertor design is proposed particularly for the large P_{heat}/R_p concept, but it will likely pose significant engineering issues such as installation of the upper divertor coil and restricted remote maintenance. In addition, accurate control of the double-null plasma configuration is required to obtain a balanced up-down divertor power distribution .

This paper reviews the steady-state power exhaust scenario and divertor design development for recent representative DEMO concepts, which were based on a plenary presentation in the 25th International Conference on Plasma Surface Interactions in Controlled Fusion Devices (PSI-25) [27]. Topics were chosen mainly from baseline DEMO design concepts for the steady-state power exhaust, which have been primarily developed for all DEMO concepts. Divertor design for the transient heat load from detached to attached plasma, and developments of the plasma design and relevant equipment for suppressing or mitigating the edge localized mode (ELM) activity are indispensable to finalize the DEMO conceptual design.

Power exhaust concepts for representative DEMO plasma designs are shown in Sec. 2. Section 3 reviews recent status of the power exhaust simulations for DEMO divertor design; simulation codes and input conditions, divertor plasma detachment, divertor geometry, tungsten (W) erosion estimation in the partially detached divertor, and effects of radial diffusion coefficients, are summarized. Engineering design concepts of water-cooled divertor, their issues of high heat removal components and coolant condition, and development of the target technologies are summarized in Sec. 4. Recent progress and key issues are summarized in Sec. 5.

2. Power exhaust concepts with impurity seeding

Power handling in the main plasma is determined by competing requirements of increasing the radiation loss fraction ($f_{rad}^{main} = P_{rad}^{main}/P_{heat}$) vs. the plasma performance as characterized by the enhancement factor of the energy confinement ($HH_{98(y,2)}$) and the normalized β (β_N). Different power exhaust scenarios were proposed for the EU-DEMO and JA-DEMO concepts. Power exhaust concepts were investigated in EU-DEMO [28] and JA-DEMO [6] from the parameter scans by the EU and JA system codes (PROCESS [29] and TPC [30], respectively). Large power exhaust scenarios require radiative cooling both in the main plasma and divertor . Relatively high-Z impurities such as argon (Ar), krypton (Kr) and xenon (Xe) are preferable for the DEMO design [31,32] in order to increase P_{rad}^{main} because of their large radiation loss rate coefficient for high T_e (>100 eV) range as shown in Fig. 2 of Reference [31]. Ar seeding was used as a reference for both DEMOs to control the radiation loss in SOL and divertor, since relatively large radiation loss is expected also at lower T_e (less than 50 eV).

EU-DEMO aims for 2-hours long pulsed operation producing net-electricity of P_{net} = 500 MW with $P_{fusion} \sim 2$ GW, which is based on the expected performance of ITER plus conservative improvements in physics and technology. Plasma parameters and the power exhaust concept of the main plasma were shown in Reference [1]: design points of the EU-DEMO (R_p = 9.0 m, $B_T \sim 6$ T) were predicted as a function of the P_{sep} ratio above the L- to H-mode transition threshold power [33] ($f_{LH} = P_{sep}/P_{LH}$) while achieving ITER-level $HH_{98(y,2)}$ (1.1) and stable β_N (2.6) by impurity seeding. Minimal R_p (9.0 m) was determined at f_{LH} = 1.2 for a given power handling parameter in the divertor (P_{sep}/R_p = 17 MWm^{-1}). The plasma density and radiation loss for the baseline design are also shown in Table 2. The EU-DEMO concept challenges increasing f_{rad}^{main} to ~0.67 by impurity seeding scenario with higher-Z impurities such as Kr and Xe, in addition to Ar to employ ITER-level power handling in the divertor, as shown in Fig. 1. Power exhaust parameters of Flexi-DEMO, i.e. $f_{rad}^{main} \sim 0.67$ and $P_{sep}/R_p \sim$ 20MWm^{-1} for the pulsed plasma and $f_{rad}^{main} \sim 0.61$ and $P_{sep}/R_p \sim$ 23 MWm^{-1} for the steady-state plasma, are also added. Such high f_{rad}^{main} was reported in the ASDEX-Upgrade (AUG) H-mode experiment with Ar and nitrogen (N) seeding [34,35], and some representative values from the database are plotted in Fig. 1. Also reducing the divertor coverage, i.e. removing the divertor baffle, is shown in Secs. 3 and 4 to increase the tritium breeding volume [36].

Table 2
Power exhaust parameters of DEMO concepts with the single null divertor.

Parameters	EU-DEMO [1]	JA-DEMO (higher-κ) [6]	CFETR (steady-state) [20]
line-ave. n_e (10^{19}m^{-3})	8.7	8.6	6.3
n^{GW} (10^{19} m^{-3})	7.2	7.3	9.1
line-ave. n_e/n^{GW}	1.2	1.2	0.67
Seeding (n_{imp}/n_e, %)	Xe (0.039) + Ar	Ar (0.6)	Ar/Ne
P_{heat} (MW)	457	435	305
P_{rad}^{main} (MW)	306	177	86
P_{rad}^{main}/P_{heat}	0.67	0.41	0.28
P_{sep} (MW)	154	258	219
P_{sep}/R_p(MWm^{-1})	17	30	30
$P_{sep}B_T/q_{95}R_pA$ (MWTm^{-1})	9.2	12.5	10.9
P_{LH} in DT(MW)	133	115	68
$f_{LH} = P_{sep}/P_{LH}$	1.2	2.2	3.2

EU-DEMO design points were investigated in Reference. [28] as *figures of merit* for handling transient heat load due to divertor plasma re-attachment and impurity concentration to achieve the divertor plasma detachment. Fig. 3(a) and (b) show the divertor operation boundaries by three thick lines and representative regions; (i) the maximum tolerable heat load condition of $P_{sep}B_T/q_{95}R_pA \sim 9$ MWTm^{-1} (q_{95}: safety factor at 95% of a_p, $A = R_p/a_p$: plasma aspect ratio), (ii) the critical impurity concentration in the SOL to produce divertor detachment ($c_{Z,det}$) comparable to a reference value (c_{REF}), which is consistent with the fuel dilution in the main plasma, and (iii) $P_{sep} = P_{LH}$. Here, the previous design value of P_{sep} = 150 MW [1] is assumed for the boundaries (i) and (ii); thus f_{LH} corresponds to 1.36 due to P_{LH} = 110 MW [28], where the reference plasma parameters were slightly revised. The normalized $c_{Z,det}$ ($\hat{c}_{Z,det}$) is used in Fig. 2 (a) and (b). Appropriate design points for the divertor operation ($P_{sep}B_t/q_{95}R_pA \leq 9$ MWTm^{-1}) and impurity concentration ($\hat{c}_{Z,det} \leq 1$) are shown within colored area (A and B), where application of the existing superconductor technology corresponds to

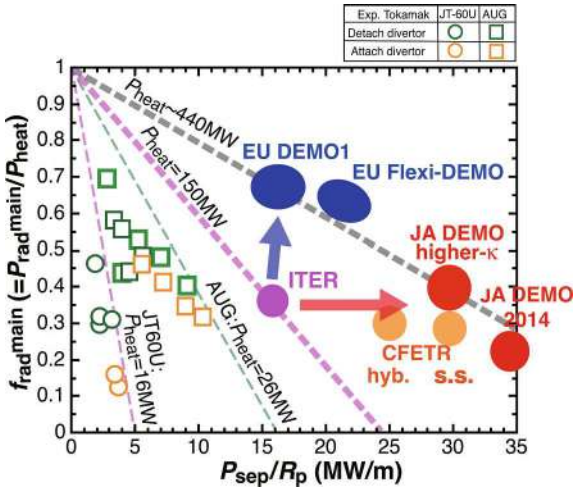

Fig. 1. Fraction of P_{rad}^{main} in the total heating power (P_{heat}) and the divertor power handling parameter (P_{sep}/R_p) for ITER, EU-DEMOs (DEMO1, Flexi-DEMO), JA-DEMOs (DEMO 2014, DEMO higher-κ) and CFETR (hybrid and steady-state concepts). Results of impurity seeding H-mode experiments in AUG [35] and JT-60U [37] are also shown by squares and circles: orange and green colors correspond to attached and detached divertor cases, respectively. (For interpretation of the references to color in this figure legend, the reader is referred to the web version of this article.)

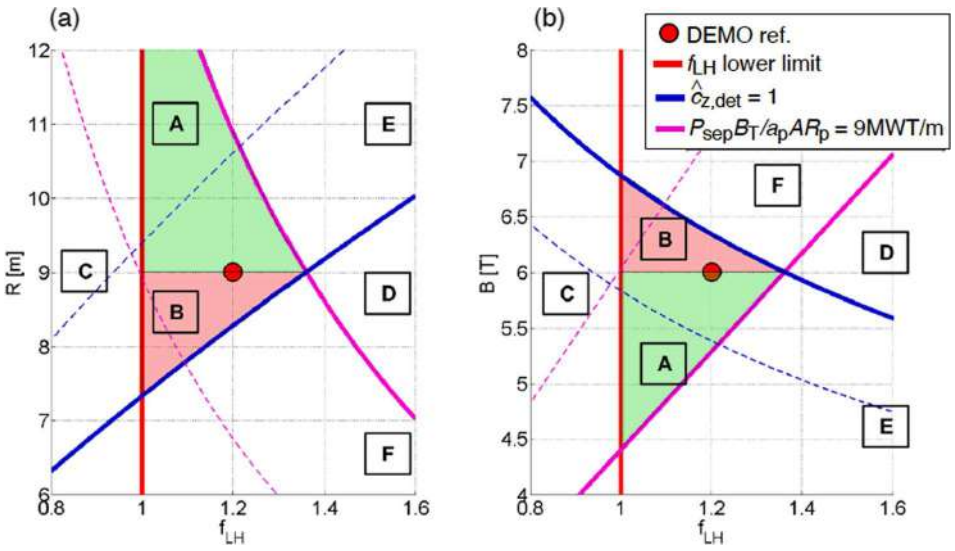

Fig. 2. Constant lines of $P_{sep}B_T/q_{95}R_pA \sim 9$ MWTm^{-1} (blue), $\hat{c}_{Z,det} \leq 1$ (magenta) and $f_{LH} = 1$ (red) in the f_{LH} - R plane (a) and $f_{LH} - B_T$ plane (b) for EU-DEMO study, assuming $P_{fusion} = 2$ GW. The reference design point is represented with a red point ($R_p = 9.0$ m, $B_T = 6$ T, $f_{LH} = 1.2$). Green shaded areas "A" identify the feasible EU-DEMO configurations, the red shaded areas "B" identify the configuration which would be feasible if advanced superconducting magnetic technology (a higher magnetic field in a smaller space than current one) is provided. C, D, E, F are not suitable for reactor operation: (C) below P_{LH}, (D) both figures of merit, (E) excessively high impurity concentration, (F) unable to deal with loss of detachment by divertor sweep and ITER-like target technology. [28]. (For interpretation of the references to color in this figure legend, the reader is referred to the web version of this article.)

"A". Provided that $f_{LH} = 1.2$ is a standard value for EU-DEMO concept, design point for updated EU-DEMO corresponds to $P_{sep}B_T/q_{95}R_pA \sim 8.11$ MWTm^{-1} and $\hat{c}_{Z,det} = 0.85$, and the exhausted power is reduced to $P_{sep} = 132$ MW. Noted that the ambiguity of P_{LH} is relatively small from the power threshold database in low Z_{eff} region (< 2) [33], which is relevent to the ITER. However, further improvement of the database with regard to impurity seeding and P_{LH} scaling for higher Z_{eff} will be necessary to determine P_{LH} more acculately for the DEMO plasma designs

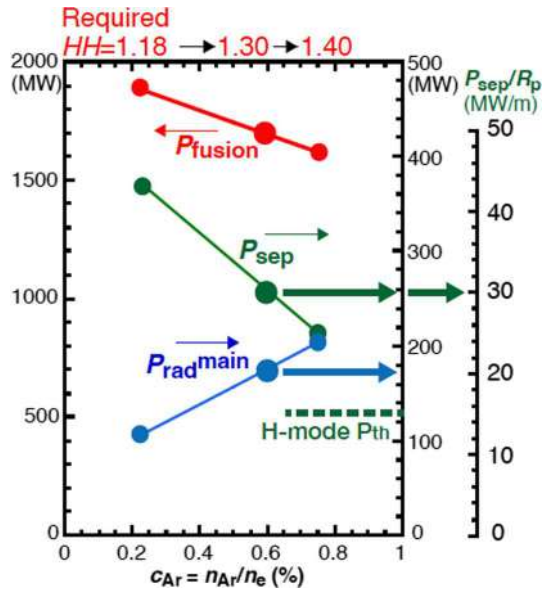

Fig. 3. P_{fusion} (red), P_{rad}^{main} (blue), P_{sep} (green) as a function of Ar impurity concentration ($c_{Ar} = n_{Ar}/n_e$) for JA-DEMO with increasing $\kappa_{95} = 1.75$. $HH_{98(y,2)}$ required for $\beta_N = 3.4$ is increased with increasing c_{Ar}. P_{rad}^{main} includes radiation loss power due to bremsstrahlung, synchrotron and impurity line radiations. Power handling parameter for the divertor (P_{sep}/R_p) is also shown at the right axis. Design point of JA-DEMO higher-κ is shown in large circles ($c_{Ar} = 0.6\%$). P_{LH} (114 MW) is shown by dotted line. [6]. (For interpretation of the references to color in this figure legend, the reader is referred to the web version of this article.)

JA-DEMO aims to steady-state operation producing P_{net} of a few 100 MW with $P_{fusion} \sim 1.5$ GW and installing enough central solenoid (CS) coils for full inductive plasma start up. High plasma density is required to achieve adequate power exhaust and low fuel dilution by impurities. For the primary plasma design (JA-DEMO 2014) as shown in Table 1, high Greenwald density fraction of $f^{GW} = \bar{n}_e/n^{GW} = 1.2$ ($n^{GW} = I_p/\pi a_p^2$ [10^{20} m^{-3}, MA, m]) was assumed, thus I_p and the line-averaged density ($\bar{n}_e$) were restricted to 12.3 MA and 7.9x10^{19} m^{-3}, respectively. Further increase of c_{Ar}^{main} reduced P_{fusion} below 1.5 GW due to the fuel dilution, and, at the same time, $HH_{98(y,2)} > 1.3$ was required. Therefore, c_{Ar}^{main}, P_{rad}^{main} and f_{rad}^{main} were restricted up to 0.25%, 82 MW and 0.22, respectively.

JA-DEMO higher-κ design (κ_{95} is increased from 1.65 to 1.75) increased I_p to 13.5 MA and $\bar{n}_e$ to 8.6×10^{19} m^{-3}, and also improved the plasma performance such as P_{fusion} and τ_E. Thus, the baseline requirements ($HH_{98(y,2)} = 1.3$, $\beta_N = 3.4$) for the steady-state JA-DEMO plasma can be obtained under the higher impurity condition of $c_{Ar}^{main} = 0.6$ %, as shown in Fig. 3 and Table 2: P_{heat} becomes comparable to that of EU-DEMO, P_{rad}^{main} is substantially increased from 82 MW (DEMO 2014) to 177 MW, and P_{sep} is reduced from 294 MW to 258 MW, which provides enough margin above P_{LH} ($f_{LH} = 2.2$). Therefore, the power exhaust concept of $f_{rad}^{main} \sim 0.4$ with $HH_{98(y,2)} = 1.3$ (both are slightly higher than ITER-level) and large P_{sep}/R_p (~30MWm^{-1}) are performance challenges for both the main plasma and divertor. The power exhaust parameters for both JA-DEMO designs are shown in Fig. 1, where some representative results of $f_{rad}^{main} \sim 0.4$ and detached divertor experiments in JT-60U long-pulse with Ar seeding were plotted [37]. Here, vertical stability of the high κ_{95} plasma was sustained by passively induced current in the conducting structures without in-vessel control coils. Increasing κ_{95} from 1.65 to 1.75 required improvements of the conducting shell design such as increasing the electrical conductance (shell width) and installing an additional shell behind the inboard breeding blankets (BBs) [38].

Since the n^{GW} values for both JA- and EU-DEMO designs are lower than that of ITER (1.1x10^{20} m^{-3}), H-mode operation with high $f^{GW} > 1$ is required to satisfy appropriate P_{fusion} and P_{net} values. On the other hand, recent experiments (JET-ILW and AUG) reported the restriction at high-f^{GW} (0.9–1) to obtain H-mode plasmas only by external gas fueling [39]. A relatively peaked profile of n_e and a pedestal density of less than n^{GW} will be necessary for the JA- and EU-DEMO plasmas to obtain the high

f^{GW}, and an internal transport barrier (ITB) of the T_e and T_i profiles as well as the n_e profile will need to be maintained, in particular, for the JA-DEMO plasma to achieve higher $HH_{98(y,2)}$ and β_N.

The plasma performance for the first target of the CFETR steady-state scenario was proposed in Reference [20], with a focus on tritium breeding; $P_{fusion} \sim 1$ GW, a stable β_N (2.0), and high $HH_{98(y,2)}$ (1.4) at relatively low $\bar{n}_e$ (6.2×10^{19} m^{-3}) and f^{GW} (0.67), which challenges the high-κ plasma design actively controlled by in-vessel coils. Power exhaust results are shown in Table 2. Power handling of large P_{sep} (219 MW) and P_{sep}/R_p (30 MWm^{-1}) is required in the divertor due to low f_{rad}^{main} (0.28), as shown in Fig. 1. Further improvement of β_N (~3.0) will achieve a high bootstrap current fraction ($f_{BS} \sim 0.75$) at a DEMO level performance of $P_{fusion} \sim 2$ GW with increasing $\bar{n}_e$ up to n^{GW}. In addition, the corresponding hybrid operation scenario with ohmic heating fraction of 0.3, aiming at reducing slightly $HH_{98(y,2)}$ (~1.2) and increasing $\bar{n}_e$ ($f^{GW} = 0.85$) for the comparable P_{fusion}, reduces P_{sep} (177 MW) and P_{sep}/R_p (25 MWm^{-1}) with the same f_{rad}^{main}.

The first phase of the K-DEMO ($R_p = 6.8$ m, $P_{fusion} = 2.2$ GW) steady-state concept was proposed to increase $f_{rad}^{main} \sim 0.4$ in order to handle the large $P_{heat} \sim 600$ MW [22] and to achieve the high plasma performance with high f_{BS}, i.e. $HH_{98(y,2)} = 1.2$, $\beta_N = 2.8$, $f_{BS} = 0.77$ [9]. The FNSF long pulse scenario proposed relatively low $f_{rad}^{main} = 0.24$ for $HH_{98(y,2)} \sim 1$, $\beta_N = 2.6$, $f_{BS} = 0.52$ [10]. While P_{sep} (360 MW for the K-DEMO and 177 MW for the FNSF) was different, P_{sep}/R_p became large (53 and 37 MWm^{-1}, respectively), which were respectively 3.3 and 2.3 times larger than that of ITER. Thus, the double-null plasma configuration was chosen for these two designs to distribute the large P_{sep} to the upper and lower divertors.

Consequently, in the recent DEMO-level power exhaust with P_{heat} of 2 – 4 times larger than that of ITER, the exhaust scenario of the large thermal power both in the main plasma and divertor is a common high priority issue. Representative concepts of increasing f_{rad}^{main} with the high plasma performance ($HH_{98(y,2)}$, β_N, f_{BS}) are summarized for the DEMO missions, which determine power handling in the divertor. At the same time, designs need to provide adequate performance for power handling and particle exhaust in the relatively low density DEMO plasmas. Design improvement to high plasma density is required from the viewpoints of reduction in the fuel dilution and the power exhaust in the main plasma and divertor.

3. Power exhaust simulation for DEMO divertor design

3.1. Divertor simulation codes and conditions

Conventional designs of DEMO divertors have been developed, based on the ITER divertor. Large power handling of $P_{sep}/R_p \sim 30$ MWm^{-1} is an important challenge for JA-DEMO and CFETR, and similar size of a long leg divertor (L_{div} = 1.6 – 1.7 m, i.e. 1.6 – 1.7 times longer than ITER) is proposed as shown in Fig. 4 (a) and (b), respectively. For the JA-DEMO divertor, the poloidal angle between the separatrix and target surface at the strike point (θ^{div}) is designed as 30° and 25° at the inner and outer targets, respectively. The flux expansion along the target, i.e. $f_{exp}^{div}/sin\theta^{div}$ where $f_{exp}^{div} = (B_p/B_T)^{mid}/(B_p/B_T)^{div}$, is similar at the inner and outer targets (~12). The divertor PFC encloses all plasma below the X-point, and the SOL field lines within the outer midplane radius (r^{mid}) of 4 cm is contacted to the inner and outer divertors. The outer target angle of CFETR is smaller than those of the JA-DEMO and ITER, thus compression of the neutral particles and efficient formation of plasma detachment will be expected particularly near the strike-point. The design concept of the ITER divertor is simplified for the EU-DEMO, i.e. baffles are removed and targets encloses near the strike-points of the long divertor leg, in order to increase the tritium breeding volume. The open and shallow geometry is considered as shown in Fig. 4(c). Instead of the dome structure, a shielding liner is installed in the private region to cover the exhaust opening against neutron flux.

Divertor plasma performance has been simulated mainly with Ar impurity seeding for DEMO. Fig. 4 also shows calculation mesh for the divertor simulations of SONIC on the JA-DEMO divertor (Ar) [14], SOLPS5.0 on the CFETR divertor (Ne or Ar) [20], and SOLPS-ITER on the EU-DEMO divertor (Ar) [17]. As will be shown in Sec. 3.3, UEDGE is used for FNSF with Ne seeding, and for K-DEMO to compare N_2, Ne and Ar seeding. Plasma cross-field drift modelling was not used (not incorporated in SONIC) for these simulation results. Studies of longer leg divertor including drifts effects on the CFETR divertor were performed by SOLPS-ITER [21], and both the inner and outer leg lengths were recently extended (1.6 m and 2.4 m, respectively). For the EU-DEMO simulation, the shielding liner is removed in this simulation work. Exhaust power (P_{out}) and particle flux were given at the core–edge boundary ($r^{mid}/a = 0.95$ for JA-DEMO and CFETR, and 0.98 for EU-DEMO); P_{out} = 250, 200, 150 MW for the above reference cases, and $P_{sep} \sim 235$, 193, 146 MW, respectively, which were slightly smaller than P_{out} since the radiation loss in the plasma edge is less than 7% of P_{out}.

Selection of the radial diffusion coefficients (diffusivities) on the ion and electron heat fluxes (χ_i, χ_e) and particle flux (D) for the SOL plasma

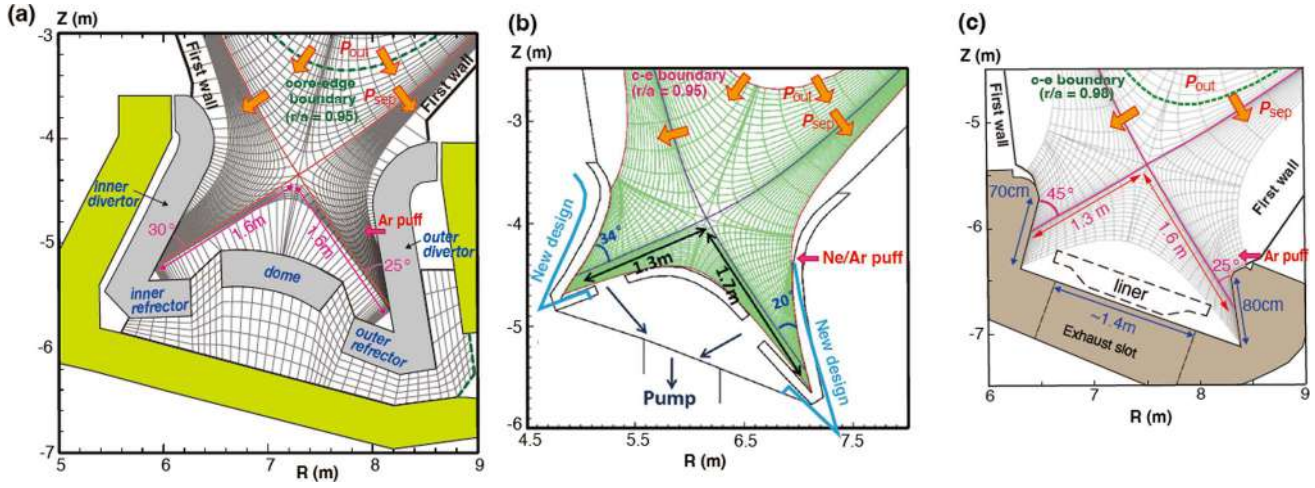

Fig. 4. (a) SONIC simulation mesh for the plasma fluid and neutral/impurity MC calculation, and the divertor geometry of JA-DEMO [14]. (b) SOLPS5.0 simulation mesh for the plasma fluid calculation, and the divertor geometry of CFETR [29]. It is used also for SOLPS-ITER simulation. (c) SOLPS-ITER simulation mesh for the plasma fluid calculation, and the divertor geometry of EU-DEMO [17].

Table 3
Power exhaust and diffusion coefficients of DEMO divertor simulation.

Parameters	EU-DEMO [17]	JA-DEMO [6,14]	CFETR [20]	FNSF[23]
Divertor code	SOLPS-ITER	SONIC	SOLPS5.0	UEDGE
P_{sep} (MW)	~ 146	~ 235	~ 193	~ 88 (lower divertor)
T_e^{sep} (keV)	0.2	0.37	0.46	~ 0.2
T_i^{sep} (keV)	0.5	0.83	2.1	~ 0.5
n_e^{sep} (10^{19} m^{-3})	2.8	2.0	1.7	~ 6
$\chi^{edge/SOL}$ (m^2 s^{-1})	0.2/ 0.18 (*1)	1.0	1.0	0.5
$D^{edge/SOL}$ (m^2 s^{-1})	0.2/ 0.42 (*1)	0.3	0.3	0.33
$\lambda_{q//}^{mid}$ (mm)	~ 3	2.9	~ 3	~ 2

Note *1: The former and latter values are provided for edge and SOL regions, respectively.

is a critical issue to simulate the divertor performance. Representative power exhaust parameters and diffusion coefficients are summarized in Table 3. For the JA-DEMO, $\chi_i = \chi_e = 1$ m^2s^{-1} and $D = 0.3$ m^2s^{-1} were the same as the "standard" values of ITER simulation by SOLPS4.3 [40]. The e-folding length near the outer midplane separatrix ($\lambda_{q//}^{mid}$) of the parallel heat flux ($q_{//}$) profile (including electron and ion components) corresponded to 2.9 mm, which was narrow compared to 3.6 mm in the ITER simulation due to higher T_e^{sep} and T_i^{sep} in the JA-DEMO (370 and 830 eV, respectively). The same $\chi = 1$ m^2s^{-1} and smaller $\chi = 0.2$ – 0.18 m^2s^{-1} were given for CFETR and EU-DEMO, respectively. While local $\lambda_{q//}^{mid}$ become small than 2 mm for the latter case, average $\lambda_{q//}^{mid}$ near the separatrix ($\Delta r^{mid} < \sim 1$ cm in SOL) is provided to similar value of ~3 mm. For the UEDGE simulation on the FNSF divertor [22], the half power of P_{sep} (0.5x176 MW) was assumed to be transported to the lower divertor and use of smaller $\chi = 0.5$ m^2s^{-1} provided smaller $\lambda_{q//}^{mid} \sim 2$ mm. On the other hand, $\lambda_{q//}^{mid}$ was estimated by $\lambda_{q//}^{Eich} = 0.7 \cdot B_t^{-0.77} \cdot q_{95}^{1.05} \cdot P_{sep}^{0.09}$ [mm, T, MW] [41] based on the experimental database of heat load profiles under the attached divertor condition, and the scaling predicted $\lambda_{q//}^{Eich} =$ 0.9 and 1.2 mm for ITER and JA-DEMO, respectively. Similar to the ITER case, $\lambda_{q//}^{mid}$ used for DEMO simulations was also wider than the empirical scaling. Reductions of both χ and D by factors of 2 and 4 produced smaller $\lambda_{q//}^{mid}$ of 1.6 and 1.2 mm, respectively, in ITER simulations [40] and the peak $q_{//}$ became larger. On the other hand, increase of the peak q_{target} remained comparatively small (20 – 40 %) due to enhancement of the particle recycling near the divertor separatrix. The influence of reducing the radial diffusion coefficients for the JA-DEMO simulation is shown and discussed in Sec. 3.5.

3.2. Plasma detachment and divertor operation at low density

A simple formula for the target heat load by the plasma (q_t^{plasma}) is described by P_{sep}, f_{rad}^{*div}, $\lambda_{q//}^{mid}$ and the flux expansion along the target ($sin\theta^{div}/f_{exp}^{div}$), as follows: $q_t^{plasma} = (P_{sep}/R_p) \cdot (1\text{-}f_{rad}^{*div}) \cdot (sin\theta^{div}/f_{exp}^{div}) \cdot (4\pi\lambda_{q//}^{mid} D^{det})^{-1}$, where the power reduction in the detachment is represented by a dissipation factor (D^{det}). Integrated divertor simulation provides a two dimensional transport solution of the plasma, neutrals and impurities in the divertor. P_{sep}, f_{rad}^{*div} and radial diffusion coefficients are important key parameters for the divertor performance. In particular, for the large P_{sep}/R_p DEMO designs, larger f_{rad}^{*div} is required compared to that of ITER (0.5–0.6). Simulation scans will determine the appropriate divertor size and geometry to maintain the large radiation peak in the divertor chamber. At the same time, n_e^{sep}/n^{GW} was reported to be ~1/3 in the H-mode plasma experiments [42,43] and a similar fraction in "standard" ITER simulations [40]. Recent experimental results in AUG W-wall and JET-ILW were also lower than critical values of 0.4 – 0.5 [44], which was predicted from the edge ballooning models, i.e. ballooning parameter formula assuming the critical ballooning parameter of 2.0 – 2.5. As a result, the operation range of n_e^{sep}/n^{GW} is expected to be 0.3 – 0.5, thus the operation boundary will be investigated in the density range of $n_e^{sep} = 2$ – 3.5×10^{19} m^{-3}, which is lower than that of ITER. Representative JA- and EU-DEMO results are mainly shown as different power exhaust concepts and divertor geometries.

Divertor operation in the low n_e^{sep} range and the influences of key parameters were recently investigated in JA-DEMO [14]. A series of n_e^{sep} scan was performed with changing fuel gas puff and divertor pumping rates (2 – 10×10^{22} Ds^{-1}), where the Ar seeding rate was controlled to keep a fixed f_{rad}^{*div} value. Two reference series for "JA-DEMO higher-κ" (Case-1: $P_{sep} \sim 235$ MW and $f_{rad}^{*div} \sim 0.8$) and "JA-DEMO 2014" (Case-2: $P_{sep} \sim 283$ MW and the same f_{rad}^{*div}), and the more severe condition with reduced f_{rad}^{*div} of ~0.7 for the two references (Case-3 and Case-4) were investigated. The power exhaust parameter above, $P_{sep} \cdot (1\text{-}f_{rad}^{*div})$, corresponds to 50, 60, 75 and 90 MW for Cases 1 to 4, respectively. Fig. 5(a) and (b) show distributions of the radiation power density (W_{rad}) in the inner and outer divertors at $n_e^{sep} = 2.0\times10^{19}$ m^{-3} for Case-1, corresponding to a near lower boundary of the n_e^{sep} range. The total radiation powers in the inner and outer divertors are comparable, i.e., 79 MW and 82 MW, respectively. The large radiation peaks near the separatrix are maintained at the upstream on both divertor legs.

In the inner divertor, a large W_{rad} is seen at 40 – 60 cm poloidally upstream of the target near the separatrix, and it is maintained far above the inner target. T_e is decreased to ~1 eV over most of the area of the target, which we describe as "full detachment", as shown in Fig. 5 (c). The total heat load (q_{target}) is evaluated by including surface recombination of the ions ($q_t^{rec} = n_i^{div} C_s^{div} E_{ion}$, where n_i^{div}, C_s^{div} and E_{ion} are ion density, sound velocity at the divertor sheath and recombination energy, respectively), radiation power load (q_t^{rad}) and neutral flux load including charge exchange and volume recombination processes (q_t^n), in addition to the plasma heat flux (q_t^{plasma}). Multi-peaks appear near the strike-point in the q_{target} profile as shown in Fig. 5 (e), which are attributed to peaks of the n_e^{div}, n_i^{div}, T_e^{div} and T_i^{div} profiles. The largest peak q_{target} of 4.2 MWm^{-2} is seen in the detached region, mostly attributed to q_t^{rec}.

In the outer divertor, a large W_{rad} is also seen at the upstream (40 – 60 cm) near the separatrix, where local c_{Ar} ($= n_{Ar}/n_i$) is increased up to 2 %. On the other hand, the W_{rad} peak shifts toward the target at the outer flux surfaces as shown in Fig. 5 (b), and it becomes smaller than 10 MWm^{-3} (lowest color bar) and located just above the target (a few cm). The plasma detachment is produced on the target within ~12 cm near the strike-point as shown in Fig. 5 (d), which we describe as "partial detachment". The peak q_{target} of 5.5 MWm^{-2} is seen at the boundary of the attached region, where both T_e^{div} and T_i^{div} are increased from ~1 eV to ~15 eV, and n_e^{div} is decreased from ~ 1.5×10^{22} m^{-3} to ~ 1.5×10^{21} m^{-3}. Thus, the peak q_{target} is sensitive to their profiles. At the same time, since the W_{rad} peak shifts toward the target, q_t^{plasma} and q_t^{rad} become dominant in the q_{target}. In the partial detachment, the peak q_{target} is sensitive to the plasma temperature and density profiles and location of the W_{rad} peak.

The outer peak q_{target} is generally larger than that of the inner peak q_{target}. Divertor operation for the outer peak q_{target} in the low n_e^{sep} range and the influences of key parameters were summarized in Fig. 6. Closed circles show a n_e^{sep} scan for Case-1, where the reference shown in Fig. 5 is marked by open circle. Squares, triangles and diamonds show other three n_e^{sep} scans for Case-2, Case-3 and Case-4, respectively. The peak q_{target} is reduced with increasing n_e^{sep}, and increased with increasing $P_{sep} \cdot (1\text{-}f_{rad}^{*div})$. As a result, Case-1 and Case-2 have acceptable solutions in the low range ($n_e^{sep} \sim 2\times10^{19}$ m^{-3}) to reduce $q_{target} \leq 10 MWm^{-2}$. On the other hand, for Case-2, the peak q_{target} is increased from 5.6 MWm^{-2} (Case-1) to 9.5 MWm^{-2} at $n_e^{sep} = 2\times10^{19}$ m^{-3} with reduced radial width of the plasma detachment to 10 cm on the target. Since the surface temperature of the W target is reduced in Case-1 (JA-DEMO higher-κ), compared to Case-2 (JA-DEMO 2014), it has advantages to provide enough operation margin to the recrystallization temperature (~1200 °C). For the lower $f_{rad}^{*div} \sim 0.7$ cases (Case-3 and Case-4), the detachment width is further decreased, and the peak q_{target} is seen also at the attached region. The peak q_{target} is further increased to 12.2 and 14.5

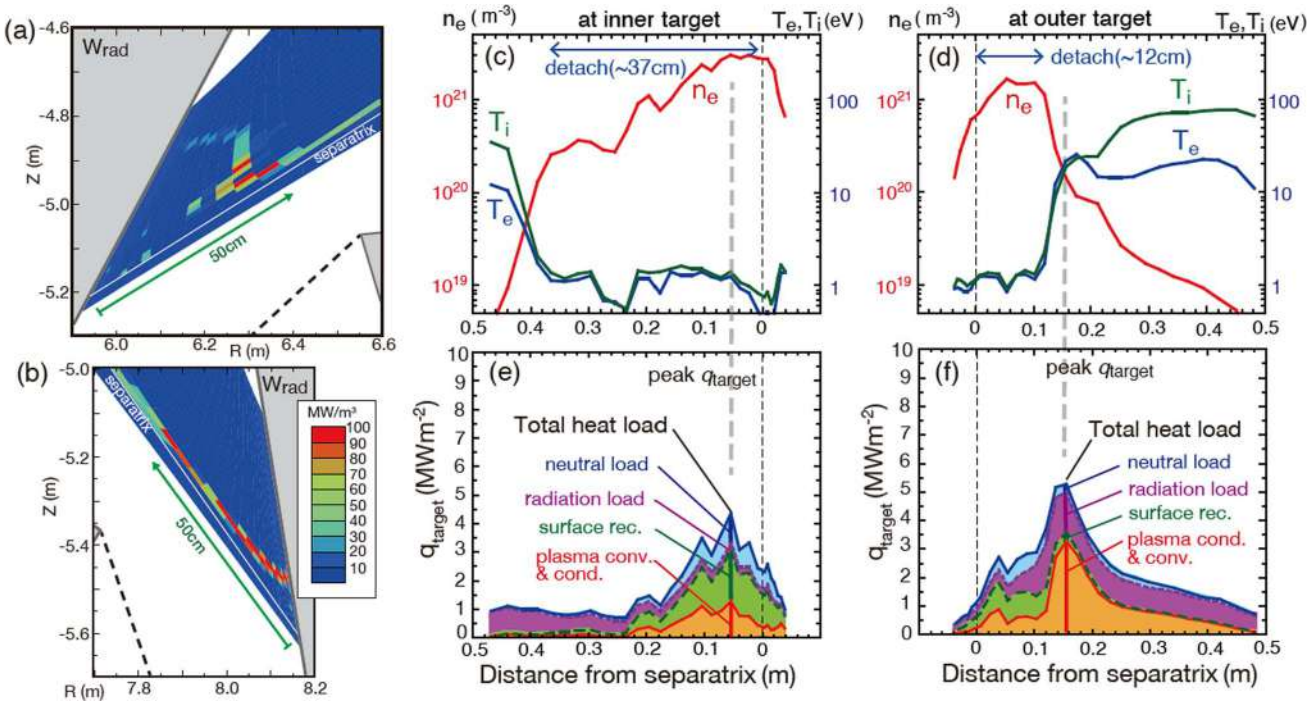

Fig. 5. (a)(b) Distributions of Ar radiation power density (W_{rad}) in the inner and outer divertors, respectively: $n_e^{sep} = 2.0 \times 10^{19} m^{-3}$, $P_{out} = 250$ MW, $P_{rad}^{edge} + P_{rad}^{sol} + P_{rad}^{div} = 200$ MW and $P_{sep} = 235$ MW. Profiles of (c) (d) n_e^{div}, T_e^{div} and T_i^{div}, (e)(f) integrating heat load components as functions of radial distance along the inner and outer divertor targets, respectively. [14].

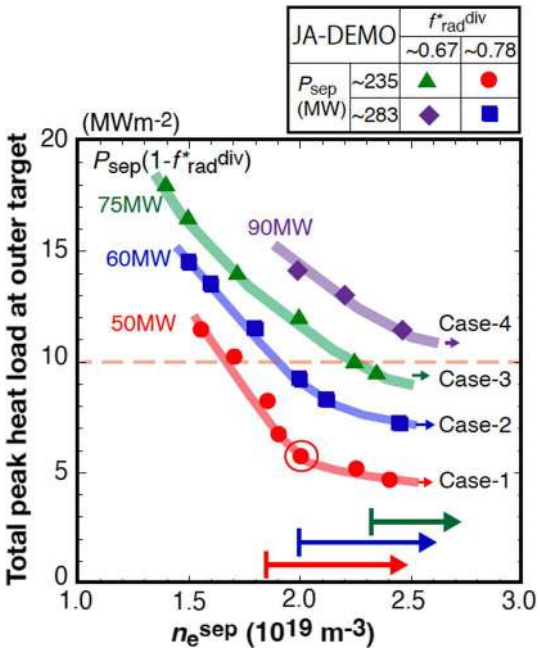

Fig. 6. Four series of peak q_{target} at the outer target for given exhaust power (P_{sep}) and radiation fraction in the SOL and divertor ($f^{*div}_{rad} = (P^{sol}_{rad} + P^{div}_{rad})/P_{sep}$) as a function of n_e^{sep} [14]. Circles and squares show Case-1 (red); JA-DEMO higher-κ reference ($P_{sep} \sim 235$ MW, $f^{*div}_{rad} \sim 0.8$) and Case-2 (blue); JA-DEMO 2014 reference ($P_{sep} \sim 283$ MW, the same f^{*div}_{rad}). Triangles (green) and diamonds (purple) show Case-3 and Case-4, respectively, i.e. lower f^{*div}_{rad} (~0.7) cases corresponding to Case-1 and Case-2, respectively. (For interpretation of the references to color in this figure legend, the reader is referred to the web version of this article.)

MWm^{-2} at $n_e^{sep} \sim 2x10^{19}$ m^{-3} due to the increase in q_t^{plasma}, where both the local T_e^{div} and T_i^{div} are increased. Higher n_e^{sep} operation (>2.3x10^{19}) is acceptable for Case-3, and further high n_e^{sep} (2.6 – 3.0×10^{19} m^{-3}) will be required for Case-4. For all cases, Ar concentrations in the midplane SOL ($c_{Ar}^{sep} = n_{Ar}^{sep}/n_e^{sep}$) are reduced to 0.4 – 1% for the range of $n_e^{sep} = 2.0$ – 2.5×10^{19} m^{-3}.

Divertor plasma performance for the EU-DEMO divertor has been investigated, using SOLPS-ITER. Reductions in T_e^{div} and q_{target} were investigated by increasing the Ar seeding rate (0.2 – 2×10^{21} Ar·s^{-1}) at relatively large gas puff rates such as an order of 10^{23} D·s^{-1}. The radiation loss distribution in the divertor, plasma profiles and accumulated heat load profiles in the inner and outer targets for the representative results are shown in Fig. 7, where $n_e^{sep} \sim 2.8x10^{19}$ m^{-3} is higher than that of the JA-DEMO and the Ar seeding rate is 1.5×10^{21} Ar·s^{-1}. P_{sep} is 146 MW, which is slightly less than P_{out} of 150 MW. Total line radiation is 75 MW, and the distribution in the divertor is shown in Fig. 7 (a). While $f^{*div}_{rad} = 0.51$, it is noted that neutral dissipation processes by charge exchange and recombination processes become 49 MW related to the large fuel gas puff. Thus, total volumetric energy loss from the plasma becomes 0.85 of P_{sep}. Large W_{rad} is seen along both the inner and outer divertor legs near the separatrix. In the inner divertor, T_e^{div} is 0.4 – 3.5 eV as shown in Fig. 7 (b): detachment ($T_e^{div} \leq 1$ eV) is produced over a substantial region. The peak q_{target} (3.2 MWm^{-2}) appears at $r^{div} \sim 3$ cm, where q_t^n becomes largest contribution near the strike-point (~1.2 MWm^{-2}) as well as q_t^{rec} (~1 MWm^{-2}). At the same time, q_t^{rad} (0.3 – 0.9 MWm^{-2}) is extended in a wide region due to large W_{rad} extended above the inner target. On the other hand, in the outer divertor, partial detachment is produced inside $r^{div} \leq 6$ cm, and T_e^{div} is increased up to 24 eV in the attached region as shown in Fig. 7 (d). It is noted that peak q_{target} (3.2 MWm^{-2}) appears in the detached region ($r^{div} \sim 4$ cm), where the local T_e^{div} is ~1 eV. Therefore, q_t^{plasma} is significantly decreased for the EU-DEMO simulation, and both q_t^{rec} (1.3 MWm^{-2}) and q_t^n (1.1 MWm^{-2}) are dominant, compared to q_t^{plasma} and q_t^{rad} (0.4 – 0.5 MWm^{-2}). These values of q_t^{plasma}, q_t^{rec} and q_t^{rad} are similar to those in the detached region of the JA-DEMO result such as at $r^{div} \sim 3$ cm in Fig. 5 (f). Since q_t^n for the EU-DEMO is 2 – 3 times larger, dissipation of momentum

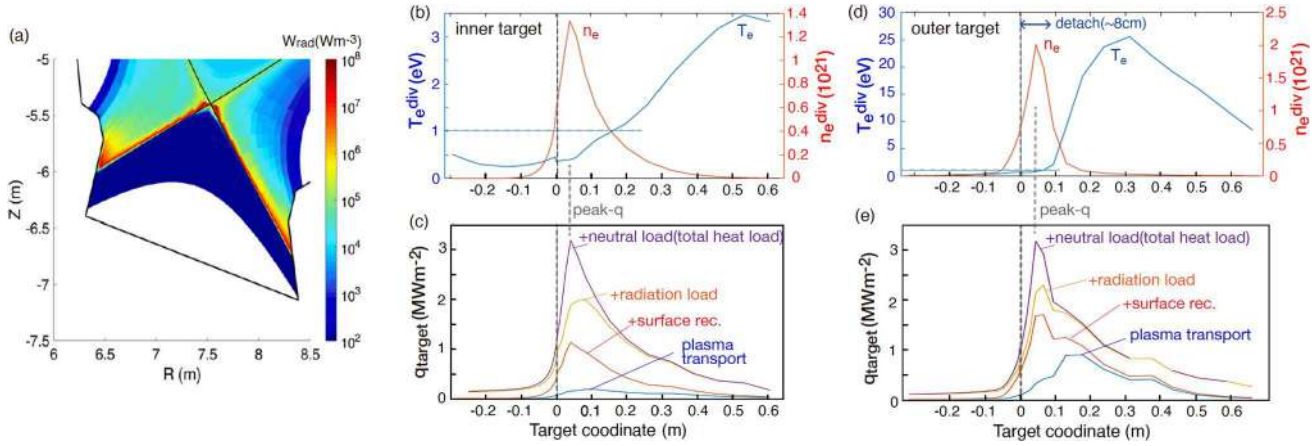

Fig. 7. (a) Distribution of line radiation power density in the divertor for EU-DEMO simulation. (b) (d) Profiles of n_e^{div} and T_e^{div}, (c) (e) Profiles of integrating heat load components at the inner and outer divertor target, respectively [17]. Radial coordinate for the heat load profiles (c) (e) is adjusted to that for the plasma profiles (b) (d). Vertical thick dotted lines correspond to the heat load peak locations, and horizontal thin dotted lines show $T_e^{div} = 1$ eV.

and ion flux may be enhanced in the EU-DEMO result. Comparison between the two divertors by either SONIC or SOLPS-ITER code, or benchmarking between SONIC and SOLPS-ITER codes in either divertor case will be required. In addition, in the EU-DEMO result, the peak q_t^{plasma} (~1 MWm^{-2}) appears in the attached region ($r^{div} = 13 - 18$ cm) similar to that in the JA-DEMO case, while local q_{target} (1.6 – 1.9 MWm^{-2}) is lower than the peak q_{target}. Since the q_t^{plasma} is sensitive to the T_e^{div} and n_e^{div} profiles in the partial detached divertor, investigation of the radial diffusion on the plasma profile is important as well as that of the plasma dissipation models.

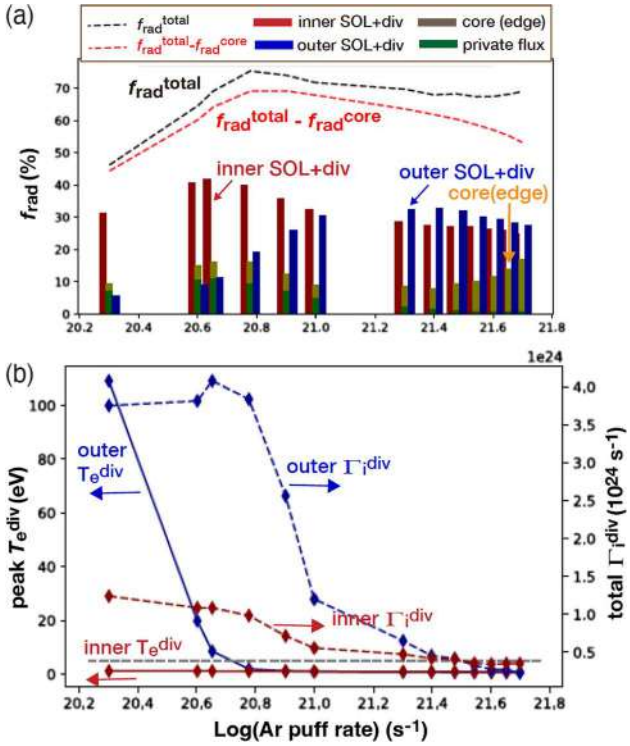

Fig. 8. (a)Vertical bars show radiation power fractions in the different plasma regions in inner SOL + divertor (dark red), outer SOL + divertor (blue), private flux (green), and core (between core–edge boundary and separatrix: dark yellow) regions, as a function of Ar seeding rate. Dotted lines show total radiation fractions of $f_{rad}^{total} = (P_{rad}^{edge} + P_{rad}^{sol} + P_{rad}^{div})/P_{out}$ and $(P_{rad}^{sol} + P_{rad}^{div})/P_{out}$. (b) Integrated ion fluxes (dash lines) and peak T_e^{div} (solid lines) at the inner and outer targets. Dark red and blue colors correspond to inner and outer SOL + divertor regions, respectively. The ion flux at the outer target begins to reduce as the peak T_e^{div} drops below 5 eV (horizontal dotted line). [19]. (For interpretation of the references to color in this figure legend, the reader is referred to the web version of this article.)

The systematic study of plasma detachment was recently performed by SOLPS-ITER code with higher $n_e^{sep} \sim 4\times10^{19}$ m^{-3} assuming larger ion flux by pellet fueling at the core–edge boundary [19]. Peak T_e^{div} at the outer target is reduced with increasing Ar seeding rate as shown in Fig. 8 (b), and the detachment in the outer divertor is produced at Ar seeding rate of 6×10^{20} Ar·s^{-1}. At the same seeding rate, the total radiation fraction (f_{rad}^{total}) also reaches the maximum as shown in Fig. 8 (a). In this study, f_{rad}^{total} is normalized by P_{out} (150 MW) and P_{rad} in the edge plasma (described as "core") is ~17 % of P_{out}, thus the maximum $f_{rad}^{total} \sim 0.75$ corresponds to f_{rad}^{*div} [= $(P_{rad}^{total} - P_{rad}^{edge})/P_{sep}$] ~ 0.70. Power loss by neutral dissipation processes is not included. Since the ion flux to the target is significantly decreased with further increasing the Ar seeding rate, large radiation loss is not maintained in the divertor region, and f_{rad}^{*div} (and f_{rad}^{total}) is gradually decreased due to increasing P_{rad} in the edge plasma. As a result, f_{rad}^{*div} is increased efficiently up to ~0.7 with increasing the Ar seeding to ~6×10^{20} Ar·s^{-1}. Further Ar seeding increases c_{Ar} and P_{rad} in SOL and edge regions, while the radiation loss in the divertor is reduced and large radiation peak is shifted towards the X-point. Thus, the detachment is enhanced both in the inner and outer divertors.

3.3. Effects of divertor geometry and drifts

Vertical target design was applied for the ITER divertor from the viewpoints of producing the plasma detachment near the separatrix at lower n_e^{sep} and the wider operation range without building up the X-point MARFE [45]. Since year-long level steady-state operation is expected for the DEMO divertor, reductions of peak T_e^{div} (and T_i^{div}) as well as the peak q_{target} are required to minimize erosion of the W-target under the partial detached divertor.

The effects of target angle (θ^{div}) on the detachment plasma and peak q_{target} were investigated in the FNSF divertor by the UEDGE code with neutral/gas fluid modelling [23]. The vertical target geometry ($\theta^{div} = 25^\circ$) was a baseline design similar to ITER, and the inner and outer L_{div} were 0.37 m and 0.60 m, respectively. Further open geometries ($\theta^{div} = 50^\circ$ and 70°), where the flux expansion at the target was decreased, were compared as shown in Fig. 9 (a). Lower divertor performance was simulated with a half power of P_{sep}, i.e. 88 MW. Thus, only the ITER-level power handling parameter ($0.5P_{sep}/R_p = 18$ MWm^{-1}) was required in the shorter leg divertor. Ne seeding was used, and relatively high n_e (1×10^{20} m^{-3}) was given at the core–edge boundary ($r^{mid}/a_p = 0.97$). The total radiation fraction by neon (Ne) and hydrogen isotopes

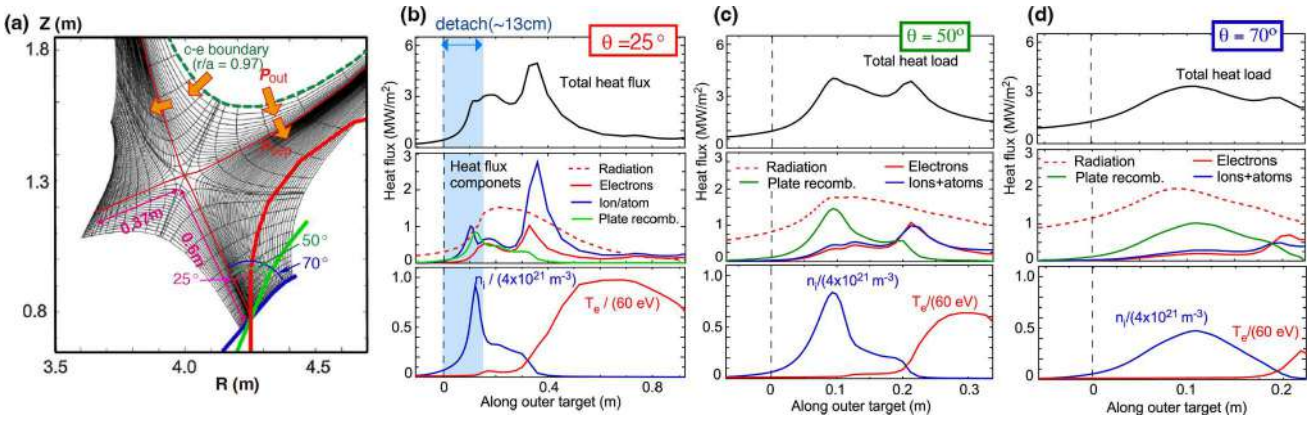

Fig. 9. (a) UEDGE calculation mesh for a baseline divertor design (vertical target geometry; $\theta^{div} = 25^{\circ}$), and other open target geometries ($\theta^{div} = 50^{\circ}$ and 70°) [23]. (b) Baseline design result at the outer target: (upper frame) total heat load along the outer divertor plate, (middle frame) heat load components of radiation, electron heat flux, ion and neutral heat flux including charge exchange and recombination processes, and surface recombination, (lower frame) profiles of electron density and temperature. Results of open target cases with poloidal angle at the strike point of (c) $\theta^{div} = 50^{\circ}$ and (d) $\theta^{div} = 70^{\circ}$ are shown.

(D/T) corresponds to $f^{*div}_{rad} = P^{div\text{-}low}_{rad}/(0.5P_{sep}) = 0.83$. For the baseline case, Fig. 9 (b) shows that partial detachment is produced at the outer target, and that low peak q_{target} (~5 MWm^{-2}) can be sustained in the attached region ($r^{div} \sim 0.3$ m), which is attributed mainly to q_t^{plasma} (~4 MWm^{-2}). Relatively high T_e^{div} of ~60 eV is seen in the outer region ($r^{div} = 0.5 - 0.7$ m) as shown in the lower plot of Fig. 9 (b). Here, heat load components by electron and ion/atom transports are separately shown in the middle plot of Fig. 9 (b), and the ion/atom transport component includes charge exchange and volume recombination processes (q_t^n). In addition, another peak q_{target} (~3 MWm^{-2}) is seen in the detach-attach boundary ($r^{div} = 0.13 - 0.25$ m), where $T_e^{div} = 2 - 3$ eV and q_t^{rad} (~1.5 MWm^{-2}) is the major heat load compared to the other components (q_t^{plasma}, q_t^n, and q_t^{rec}) due to significant radiation peak near the target. It was noted [23] that kinetic transport modelling of neutrals and molecules (self-consistent coupling of the UEDGE and DEGAS codes) is required for accurate evaluation, which would be expected to extend the low T_e^{div} region and further reduce the peak q_{target}.

For the open geometry cases ($\theta^{div} = 50^{\circ}$ and 70°), the detached region becomes radially wider, and the peak q_{target} at the attached region is reduced due to reduction in T_e^{div} (and T_i^{div}) as shown in Fig. 9 (c) and (d). For both cases, q_t^{rad} is also the major heat load component. For the case of $\theta^{div} = 50^{\circ}$, the peak q_{target} in the detach-attach boundary ($r^{div} =$ 0.10–0.18 m) is increased due to increase in q_t^{rec}, and the two peak q_{target} values are comparable (~4 MWm^{-2}). For the case of $\theta^{div} = 70^{\circ}$, the detached region is widely extended to $r^{div} \sim 0.18$ m, and T_e^{div} and T_i^{div} are further reduced to less than 1 eV. A broad q_{target} peak (~3.5 MWm^{-2}) is seen near $r^{div} \sim 0.1$ m, where q_t^{rad} (~1.8 MWm^{-2}) is the major heat load, then $q_t^{rec} \sim 1$ MWm^{-2}, and q_t^{plasma} is reduced to ~0.7 MWm^{-2}. It is similar to the inner divertor (nearly full detachment). The operation window of wide detachment and low q_{target} is important for the choice of the divertor geometry. At the same time, transport modelling of dissipation processes, elastic collisions and kinetic effects become important to evaluate the peak q_{target} and the impurity distribution in the nearly fully detached divertor. Further studies will continue using self-consistent simulation of the UEDGE and DEGAS2 codes.

Appropriate divertor leg length (L_{div}) for the vertical target design is primarily determined to maintain the seeding impurity and large radiation peak in the divertor. Divertor performance with $L_{div} = 1.6 - 1.7$ m has been investigated for the high P_{sep}/R_p handling such as JA-DEMO (30 – 35 MWm^{-1} by Ar seeding) [14,15] and CFETR (28 MWm^{-1} by Ne seeding) [20], and these results were demonstrated to be appropriate for their reference design. Further study was recently performed for the CFETR by SOLPS-ITER with various drifts activated such as$\nabla B \times \boldsymbol{B}$ and $\boldsymbol{E} \times \boldsymbol{B}$, which produced inboard-enhanced asymmetry of the particle flux profile and outboard-enhanced heat load profile for the normal B_T direction, i.e. ion∇B drift towards the divertor [21]. Extension of L_{div} was proposed, and effects on the plasma detachment and impurity retention in the divertor were investigated. Geometries of the refence and longer leg divertors are shown in Fig. 4 (b) and 10 (a): both inner and outer L_{div} were extended from 1.3 m and 1.7 m to 1.6 m and 2.4 m, respectively. Here, inner θ^{div} was increased from 34° to 46°, and outer θ^{div} was the same (20°) [46]. P_{out} from the core–edge boundary was the same (200 MW) as the previous study, but radial distributions of χ and D were introduced, where χ was reduced to 0.5 m^2s^{-1} inside the separatrix ($r^{mid} =$ -5 – 0 cm) and increased to 2.0 m^2s^{-1} in the far SOL region ($r^{mid} = 3 - 6$ cm): D was similarly varied. Typical $\lambda_{q//}^{mid}$ was ~4 mm and $n_e^{sep} = 3.7\times10^{19}$ m^{-3} in the series of calculations. Comparison between Ne and Ar seedings showed that divertor cooling by the Ar seeding was efficient, thus the Ar seeding was chosen for the baseline scenario.

Under a comparable conditions for the gas puff (4×10^{22} D·s^{-1}) and Ar seeding (4×10^{19} Ar·s^{-1}) with drifts activated, the poloidal distributions of T_e and c_{Ar} near the separatrix from the outer midplane SOL to the target for the two leg length cases are compared in Fig. 10 (b) and (c), respectively. For the reference case, the target plasma becomes attached ($T_e^{div} = 230$ eV) due to lower radiation loss in the outer divertor, while T_e^{div} is significantly reduced to ~3 eV for the longer leg case. Next, similar poloidal distributions of T_e are achieved with increasing Ar seeding (1×10^{20} Ar·s^{-1}) only for the reference case as shown in Fig. 10 (d) and (e), where $f^{*div}_{rad} \sim 0.7$ is comparable and similar partial detachment ($T_e^{div} \sim 1$ eV) is produced near the separatrix (Fig. 10 (f) and (g)). For the longer leg case, peak T_e^{div} at $r^{div} \sim 0.35$ m in the attached region is reduced from 47 eV (reference case) to 34 eV while reduction in the peak q_{target} is small. As a result, drifts will affect the divertor performance, i.e. more severe heat load and higher peak T_e^{div} at the outer divertor, the longer leg is considered as new baseline design in order to reduce both the peak q_{target} and T_e^{div}, to produce required c_{Ar} in SOL and edge regions, and to extend the divertor operation window at lower n_e^{sep}.

Reduction in the peak q_{target} by N_2, Ne or Ar seeding was investigated in the double-null divertor for K-DEMO (by UEDGE) [22] with ITER-level leg length and larger power to either divertor, i.e. $0.5P_{out} = 300$ MW. Results showed that Ar seeding enhanced partial detachment more than Ne and N_2 cases, and the peak q_{target} was efficiently reduced. It is noted that appropriate power handling ($q_{target} \leq 10$ MWm^{-2}) was achieved only by reducing the pumping speed, i.e. increasing the albedo of the divertor pumping to 0.99945. Since the operation window of the detachment is limited, further improvements of the geometry and the power exhaust scenario both in the main plasma and divertor will be required.

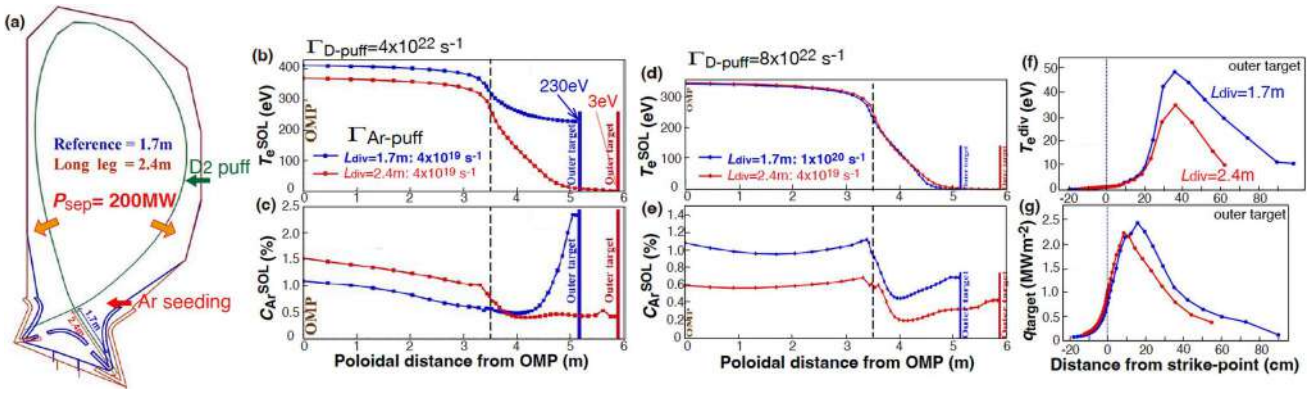

Fig. 10. (a)Baseline (reference) and long leg divertor geometries for CFETR. SOLPS-ITER simulations with various drifts activated such as$\nabla B \times \boldsymbol{B}$ and $\boldsymbol{E} \times \boldsymbol{B}$ [21]. Comparisons of poloidal profiles (starting from the outer midplane down to outer target) of (b) electron temperature (T_e^{SOL}) and (c) Ar concentration (c_{Ar}^{SOL}) near the separatrix ($r - r_{sep} = 0.1$ cm mapped to OMP), for the reference and long leg divertors. For both cases, D_2 gas injection rate and Ar seeding rate are 4.0×10^{22} and 4.0×10^{19} atom s^{-1}, respectively. Comparisons of poloidal profiles of (d) T_e^{SOL} and (e) $c_{Ar}{}^{SOL}$ near the separatrix from the OMP to outer target with the same Ar seeding rate and D_2 gas injection rate of 8.0×10^{22} atom s^{-1}. Ar seeding rate for reference divertor and longer leg divertors are 1.0×10^{20} and 4.0×10^{19} atom s^{-1}, respectively. Corresponding radial profiles of (f) T_e^{div} and (g) total heat load (q_{target}) along the outer target.

3.4. Estimation of steady-state W-erosion in the partial detachment

Net erosion of the W target becomes a life-time issue for the DEMO divertor since the ion fluence is expected to be one order of magnitude larger than that in ITER. Low T_e^{div} and T_i^{div} plasma is preferable in the partially detached divertor, in particular, for the vertical target geometry. W-flux sputtered from the target was reported in addition to the divertor plasma parameters of EU-DEMO [17], JA-DEMO [14], CFETR [20] and FNSF [23], where these estimations were carried out by different methods. W-sputter flux and simple estimation of the erosion rate are summarized in Table 4. Here, effects of transient plasma flux such as mitigated ELMs are not included as we described in Sec. 1. W-erosion is enhanced mainly by seeding impurity at the attached region, where the local T_e^{div} is increased to 20 – 40 eV while the incident ion flux (Γ_i^{div}) is reduced at the outer r^{div}. Gross W-sputter flux in the DEMO divertor simulation is sensitive to local plasma condition of Γ_i^{div} and impurity concentration (c_z) as well as T_e^{div}. Typical values of gross W-sputter flux (Γ_W^{div}) are reported to be a wide range between 6.3×10^{17} and 8×10^{19} W·m^{-2}s^{-1}, where the TRIM code surface database [47] was used for the EU-DEMO result (the small one) and the DIVIMP code (including prompt redeposition and self-sputtering of W) [48] was applied to the CFETR (the high one). For the JA-DEMO case, Γ_W^{div} was determined mostly by Ar impurity ions, and it was defined as yields per impacting hydrogen ion ($Y_Z \cdot c_z \cdot \Gamma_i^{div}$) [42], where the incident energy for the sup-pering yield (Y_Z) was given by the typical charge state (Z), plasma temperatures and the sheath potential, i.e. $2Z \cdot T_i^{div} + 3T_e^{div}$. For the FNSF case, Y_Z was calculated by the incident plasma ions (D/T) with the temperatures and the sheath potential, i.e. ($2T_i^{div} + 3T_e^{div}$) [49].

Net erosion rate is estimated by a simple formula of Δd_{sec} (nm/s) = $10^3 \cdot R_{net} \cdot \Gamma_W^{div} / [6.02\times10^{26}/183.8 \cdot \rho] = 1.57\times10^{-20} R_{net} \cdot \Gamma_W^{div}$, where R_{net} is the ratio of net to gross erosion rate and ρ is W mass density (19.3×10^3 kgm^{-3}). R_{net} is also a critical factor, and 0.1 is given for the FNSF estimation, which considers prompt redeposition (finite-Larmor) effect [50]. The same R_{net} is assumed for the EU-DEMO and JA-DEMO cases, and lower value of 0.03 is evaluated by DIVIMP calculation for the CFETR case. Prompt and local deposition modelling such as the finite-Larmor effect and friction force by the plasma flow, and an experiment database for gross to net erosion ratio are urgently needed. Net erosion depth for year-long operation is also estimated as Δd_{year} (mm/year) = $4.95\times10^{-19} R_{net} \cdot \Gamma_W^{div}$, which is an order of magnitude larger than that of ITER (e.g. assuming ITER with 2500 pulses of 400 s discharges per year). Some results suggest that Δd_{year} reaches the 1 mm-level, which corresponds to 10 – 20% of the monoblock thickness. As a result, simulation results in the vertical target geometry suggested further reduction of both peak T_e^{div} and T_i^{div}, such as "pronounced detachment" reported in ASDEX-upgrade [35], where the peak $T_e^{div} \sim 5$ eV in the partially attached region, is preferable. Operation at higher n_e^{sep} and/or sweep of the strike-point location [28,51] will need to be considered.

Table 4
Estimation of W erosion depth at the peak T_e^{div} by seeding impurities.

	EU-DEMO [17]	JA-DEMO [6,14]	CFETR [20]	FNSF[23]
T_e^{div} *at* r^{div} (attached region)	20 eV at 40 cm	25 eV at 20 cm	20 eV at 45 cm	40 eV at 45 cm
Γ_i^{div} (m^{-2}s^{-1})	~ 10^{21}	4×10^{22}	5×10^{21}	~ 10^{22}
$c_Z = n_Z/n_i$ (%)	1 (Ar)	0.4 (Ar)	0.6 (Ne)	0.4 (Ne)
Γ_W^{div} (m^{-2}s^{-1})	6.3×10^{17} (*1)	1.9×10^{19}	8×10^{19}	7×10^{18}
Net erosion ratio: R_{net}	0.1	0.1	0.03 (*2)	0.1 (*3)
Δd_{sec} (nm s^{-1})	~ 0.001	0.03	0.04	0.011
Δd_{year} (mm year^{-1})	~ 0.03	~ 0.9	~ 1.2	~ 0.3

Note *1: calculation is performed using the TRIM database [47].
Note *2: Ratio is evaluated by DIVIMP calculation [48].
Note *3: prompt re-deposition reduction factor is chosen from [50].

3.5. Effects of radial diffusion coefficients on power exhaust

In the divertor simulation, the radial diffusion coefficients of the SOL plasma are primary key parameters to determine profiles of the heat and particle fluxes. For the recent DEMO simulations, $\lambda_{q//}^{mid}$ of the total (electron and ion) $q_{//}$ profile was within a range of 2 – 3 mm, while different diffusion coefficients were used as shown in Sec. 3.1 and Table 3. The effects of smaller $\lambda_{q//}^{mid}$, which was produced by reducing diffusion coefficients, on the partial detachment and divertor operation were investigated in JA-DEMO [14,15]. Some representative simulations with both χ and D reduced to half values, i.e. $\chi_e = \chi_i = 0.5$ m^{2}s^{-1} and $D = 0.15$ m^{2}s^{-1}, were performed for the four series shown in Sec. 3.2. Profiles of electron, ion and total parallel heat fluxes near the X-point ($q_{//e}^{Xp}$, $q_{//i}^{Xp}$ and $q_{//e}^{Xp} + q_{//i}^{Xp}$) for Case-1 ($P_{sep} \sim 235$ MW, $f_{rad}^{*div} \sim 0.8$ and the same n_e^{sep} of 2.0×10^{19} m^{-3}) are compared in Fig. 11 (a) and (c), mapping to the outer midplane radius (r^{mid}). Here, radial gradients of T_e^{Xp}, T_i^{Xp} and n_e^{Xp} profiles were generally increased for the reduced χ and D case, and the increase in T_i^{Xp} (from 820 to 1190 eV for the same n_e^{sep} cases) was significant due to reduction in n_e^{Xp} in the SOL region. Both $q_{//e}^{Xp}$ and $q_{//e}^{Xp} + q_{//i}^{Xp}$ profiles are described approximately by a two-exponential function such as $q_{//}(r^{mid}) = q_{//}^{near} exp(-r^{mid}/\lambda_{q//}^{near}) + q_{//}^{far} exp(-r^{mid}/\lambda_{q//}^{far})$, where $\lambda_{q//}^{near}$ and $\lambda_{q//}^{far}$ are e-folding lengths of "near-SOL" and